

On the Use of Discrete Cosine Transforms for Multicarrier Communications

Fernando Cruz-Roldan, Maria Elena Dominguez-Jimenez,
Gabriela Sansigre Vidal, Pedro Amo-López,
Manuel Blanco-Velasco, and Angel Bravo-Santos

Abstract—In this correspondence, the conditions to use any kind of discrete cosine transform (DCT) for multicarrier data transmission are derived. The symmetric convolution-multiplication property of each DCT implies that when symmetric convolution is performed in the time domain, an element-by-element multiplication is performed in the corresponding discrete trigonometric domain. Therefore, appending symmetric redundancy (as prefix and suffix) into each data symbol to be transmitted, and also enforcing symmetry for the equivalent channel impulse response, the linear convolution performed in the transmission channel becomes a symmetric convolution in those samples of interest. Furthermore, the channel equalization can be carried out by means of a bank of scalars in the corresponding discrete cosine transform domain. The expressions for obtaining the value of each scalar corresponding to these one-tap per subcarrier equalizers are presented. This study is completed with several computer simulations in mobile broadband wireless communication scenarios, considering the presence of carrier frequency offset (CFO). The obtained results indicate that the proposed systems outperform the standardized ones based on the DFT.

Index Terms—Carrier-frequency offset (CFO), discrete cosine transform (DCT), discrete multitone modulation (DMT), multicarrier modulation (MCM), multicarrier transceiver, orthogonal frequency-division multiplexing (OFDM).

I. INTRODUCTION

A general block diagram to implement multicarrier modulation (MCM) is shown in Fig. 1. At the transmitter, the incoming data are processed by an N -point inverse transform ($T_{J^{-1}}$), with N being the number of subchannels or subcarriers. At the receiver, a discrete transform (T_c) is also performed. Discrete multitone modulation (DMT) and orthogonal frequency-division multiplexing (OFDM) are particular forms of multicarrier modulation (MCM) [1], and they have been the modulation choice for fixed and nomadic broadband communications (see e.g. [2]-[5]). In mobile communications, OFDM has also been adopted in WiMAX [6], LTE downlink [7], and in the physical layer of 802.11p that describes the wireless access in vehicular environments (vehicle-to-vehicle (V2V) communications) [8]. In DMT and OFDM, the $N \times N$ matrices T_a and T_c are carried

TABLE I
DEFINITIONS FOR THE DISCRETE COSINE TRANSFORMS EVEN AND ODD [16]

DCT even	DCT odd
$(C_{1e})_{k,j} = \frac{1}{2} \cos \left(\frac{\pi}{2} (k + \frac{1}{2}) (j + \frac{1}{2}) \right), 0 < k, j < N$ $a_0 = 1/2 = a_N, c_{ij} = d_{ij} \pm 0, N$	$(C_{1o})_{fc,j} = 2a_j \cos \left(\frac{\pi}{2} (j + \frac{1}{2}) fc \right), 0 < k, j < N - 1$ $a_0 = 1/2, a_j = 1, j \neq 0$
$(C_{2eh})_{k,j} = 2 \cos \left(\frac{\pi}{2} (2j_2 + 1)^2 r \right), 0 < k, j < N - 1$	$(C_{2o})_M = 26_{fc} \cos \left(\frac{\pi}{2} (j + \frac{1}{2}) fc \right), 0 < fc, j < JV - 1$ $6_{fc} = 1, \wedge \wedge \wedge - 1, 6 \wedge - 1 = 1/2$
$(C_{3e})_M = 2aj \cos \left(\frac{\pi}{2} (fc \wedge j) r \right), 0 < fc, j < JV - 1$ $a_0 = 1/2, a_j = 1, j \neq 0$	$(C_{3o})_M = 2a_j \cos \left(\frac{\pi}{2} (j + \frac{1}{2}) fc \right), 0 < fc, j < JV - 1$ $a_0 = 1/2, a_j = 1, j \neq 0$
$(C_{4e})_M = 2 \cos \left(\frac{\pi}{2} (fc + 1) (j + 1) \right), 0 < fc, j < JV - 1$	$(C_{4o})_M = 2 \cos \left(\frac{\pi}{2} (fc + 1) (j + 1) \right), 0 < fc, j < JV - 1$

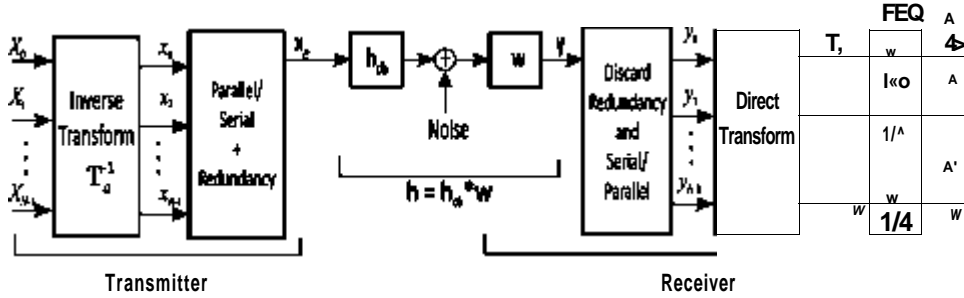


Fig. 1. Block diagram of a transforms-based multicarrier system over a channel with additive noise.

out using Discrete Fourier Transforms (DFTs) implemented by fast algorithms.

Discrete Fourier transform (DFT)-based systems are efficient to fight against multi-path fading channels, but they present some drawbacks, as a high peak-to-average power ratio, or the sensitivity to carrier-frequency offsets (CFO). Frequency offset interferences are mainly caused in mobile OFDM communications by mismatch or ill-stability of the local oscillators in the transmitter and the receiver, and by the movement-induced Doppler shift. As a well-known fact, the broadening of the Doppler spectrum caused by the speed of the terminal is a main effect that has a direct impact on the bit error probability (BEP).

Different solutions to correct CFO and the rest of drawbacks are based on the use of discrete trigonometric transforms (DTTs), mainly discrete cosine transform (DCT) Type-II even,¹ as multicarrier modulators [10]–[15]. Due to the energy-compaction of DCT, there is less ICI leakage to adjacent subcarriers in DCT-MCM than in DFT-MCM, and this results in better performance robustness to frequency offset [13], [14]. Moreover, the anti-symmetry introduced in DCT-MCM enables the full range of frequency offset estimation, and this leads to more accurate and more robust estimation [15].

In this work, we address the design of multicarrier transceivers employing any kind of DCT at both the transmitter (T_d^{-1}) and the receiver (T_c) sides. This problem can be formulated in two different ways. The first one consists in deriving the conditions to use any kind of DCT for multicarrier data transmission using matrices. Let us consider the system of Fig. 1, in which a left prefix and also a right suffix are introduced as redundancy into each data x to be transmitted: $x_e = [x/p \ x \ x/rs]$. The goal of these prefix x/p and suffix x/rs is to obtain a

¹Eight different types of DCTs (see Table I) and also eight types of DSTs are shown in [9].

channel matrix H perfectly diagonalizable by DCTs. Then, using the diagonalization properties of DCTs shown in [9], the frequency-domain equalizer at the receiver is reduced to a simple structure. The above matrix formulation was employed in [13], [17] to obtain the conditions for using the DCT Type-II even (DCT2e) and DCT Type-III (even and odd) in the MCM context.

The second way of formulating the use of DCTs for multicarrier data transmission is based on the interpretation of the symmetric convolution. That is, if DCTs are used as block transforms in the system of Fig. 1, the idea consists in some way forcing the linear convolution performed by the channel to become a symmetric convolution in the time-domain, or equivalently, an element-by-element operation in the corresponding DCT domain. In this regard, Martucci shows in [16] that DCTs also have the convolution-multiplication property, and the result of symmetric convolution in time-domain is the same as that obtained by taking an inverse DCT of the pointwise product of the forward DCTs of those two sequences. So, taking advantage of the convolution-multiplication property of each DCT, we find an efficient form of equalizing the effects of the transmission channel by means of one-tap per sub-carrier equalizer. In this work, the above formulation is used to obtain the conditions for using the eight different DCTs for multicarrier data transmission.

Therefore, this work complements the results obtained in previous studies for DCT2e [13], [14] and DCT3 [17]. Since there are objective reasons to use DCT as an alternative to DFT for multicarrier communications (see e.g. [13]), the goal of our study is focused on deriving the conditions to design the system of Fig. 1 with the eight different types of DCTs. One key contribution of this work is to define the kind of redundancy to be introduced into each data symbol to be transmitted, along with the symmetry to be imposed on the channel impulse re-

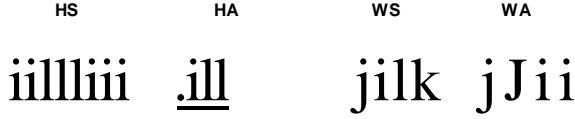


Fig. 2. Examples of symmetry types.

TABLE II
SOME TYPES OF SYMMETRIC CONVOLUTION [16]

Row	$(e_a^s c \ \ell b)$	$(T_a^s c T_b)$	$r \wedge n$
1	$(WSWS^s_c \ WSWS)$	$(C_{le}^s c C_{le})$	$r \wedge 1$
2	$(HSHS^s_c \ WSWS)$	$(C_{2e}^s c C_{le})$	C_s
3	$(WSWA^s_c \ WSWA)$	$(C_{3e}^s c C_{3e})$	$c \wedge 1$
4	$(HSHA^s_c \ WSWA)$	$(C_{4e}^s c C_{3e})$	C_{je}^1
5	$(WSHS^s_c \ WSHS)$	$(C_{lo}^s c C_{lo})$	$r \wedge p$
6	$(HSWS^s_c \ WSHS)$	$(C_{2o}^s c C_{lo})$	C_s
7	$(WSHA^s_c \ WSHA)$	$(C_{3o}^s c C_{3o})$	C_s
8	$(HSWA^s_c \ WSHA)$	$(C_{4o}^s c C_{3o})$	$1cZ^1$

sponse² by means of the front-end filter w . As it is known, the introduction of redundancy helps to equalize the transmission channel more easily. The second key contribution is to derive the expressions to obtain the coefficients that perform the frequency domain equalization by means of a one-tap equalizer.

The remainder of this paper is organized as follows. In Section II, the convolution-multiplication properties of symmetric convolutions in different DCTs domains are presented. These properties are used to widen the list of possible DCTs to be used for multicarrier data transmission. In Section III, it is demonstrated that the proposed results are consistent with other published works. Then, several examples are included in Section IV to illustrate the benefits of the proposed DCT-MCM versus DFT-MCM. The performance of DCT Type-IV (DCT4) and OFDM systems over different communication scenarios is also evaluated, including channels with the three basic Doppler spectrum: round, flat and classic [18]. We have chosen a power delay profile typical of an urban environment for the channels. Finally, Section V contains some concluding remarks.

II. DISCRETE COSINE TRANSFORM FOR MULTICARRIER MODULATION

The list of possible DCTs for using in MCM data transmission can be widened to the eight different DCTs reported in [9] and defined in Table I. In this section, there is an explanation of how to do it, considering the symbol data length satisfies the following condition: $N > (2v + 1)$, which is the case of interest to avoid significant guard overhead.

²As in [13], [17], only symmetric channel filters h ($h_{-k} = h_k$, $k = 1, \dots, u$) are considered throughout this work. This requirement can be met in practice by means of the front-end filter w , which is commonly used in DFT-based MCMs. Remind that frequency domain channel equalization is easy to be performed in OFDM/DMT when the cyclic prefix length is at least the order L of the transmission channel impulse response. However, this requirement is often restrictive, especially at high sampling rates, where the channel order can extend into many hundreds of samples. In order to overcome this problem, the pre-filter w is placed at the receiver in cascade with the channel to produce an effective shortened impulse response, optimally squeezing the channel energy into a time-frame of less than $L + 1$ samples [19]. Different solutions to meet the symmetry condition are proposed in [13, p. 915].

Let us consider four different types of symmetry in a sequence [16]: whole-sample symmetry (WS), whole-sample antisymmetry (WA), half-sample symmetry (HS), or half-sample antisymmetry (HA). Fig. 2 shows examples of each one of the above sequences. In [16], the convolution-multiplication properties of the eight types of DCTs, the eight types of DSTs, and also forty different types of symmetric convolution are reported. Table II summarizes some of the results included in [16] for general digital signal processing; s_a and Sb mean the symmetric extension operators applied to each sequence to be convolved, and T_a and T_b are the DTTs that must be taken in the first sequence and in the right-half samples of the second one, respectively. Finally, T^{-1} is the appropriate inverse transform which relates the convolution-multiplication domains.

The interpretation of Table II in the MCM context is as follows. The symmetries in s_a establish the prefix and the suffix that have to be inserted in the transmitted sequence x . On the other hand, since we assume that $N \gg (2^v + 1)$, only the first symmetry in Sb is considered to obtain h . The third column in Table II indicates the domain(s) or transform(s) where the symmetric convolution is solved by an element-by-element multiplication. Observe that in the MCM context the inverse of T_a is related to the block transform used as transmitter, and T_b is indicating the DTT to obtain the $N d_i$ coefficients from the $(v+1) \times 1$ or $(7v+1) \times 1$ column vector h'_{zp} , which is the filter-right-half $h^T = [h_0, h_1, \dots, h_v]$ extended by zero-padding to N or $N + 1$ samples. Finally, the fourth column of Table II indicates the inverse of the transform used at the receiver.

To sum up, Table III shows the interpretation of Table II in the MCM context. Special attention must be paid to the length of the T^{\wedge} transform since in some cases it must be $N + 1$ (C_{ie} or C_{3o} in the second or the last row of Table III respectively), whereas for the rest of cases this length must be N .

III. CONSISTENCY WITH PREVIOUS RESULTS

A. DCT-IIe-Based MCM

In [13], the discrete cosine transform type-II even (DCT2e or C_{2e})-based multicarrier modulator transceiver is derived. Basically, it can be obtained from the block diagram of Fig. 1 as follows:

- (i) Inverse transform T^{-1} : IDCT2e ($N \times N$ matrix C^{-1}).
- (ii) Parallel-to-serial converter, including a prefix

$$(x/p)_n = X_{-i-p} \quad 71 = 0, \dots, -i > -1,$$

and also a suffix:

$$(X_{rs})_n = X_{N-l-n}, \quad n = 0, \dots, \&' - 1.$$

- (iii) A front-end-prefilter w that imposes the symmetry condition ($h-k = hk$, $k = 1, \dots, v$) in the equivalent impulse response $h = h_c h * w = [h_{-v}, \dots, h_{-i}, h_0, h_1, \dots, h_v]$. For channels with long memory (longer than $2v + 1$), this front-end prefilter also has to produce an effective shortened impulse response. Once h is obtained, a filter-right-half is defined as $h^T = [h_0, h_1, \dots, h_v]$.
- (iv) Selection of the corresponding N samples of interest, and serial-to-parallel converter.
- (v) Direct transform T_c : DCT2e ($N \times N$ matrix C_{2e}).
- (vi) FEQ block: Frequency-domain equalizer, in which the numbers d_i are given by [13, p. 917]

$$\hat{e} \wedge C \wedge . e \wedge \ell = 0, \dots, JV - 1, \quad (1)$$

$$e^{*+1} C_{2(i)ei}$$

TABLE III
INTERPRETATION OF SYMMETRIC CONVOLUTION (TABLE II) IN THE MCM CONTEXT

Row	Symmetry in x_a	Prefix	Suffix	Symmetry in e_b	Symmetry in h ($A \wedge > (2i/+1)$)	Transmitter	Receiver
1	WSWS	$\%v - n$ $Vn = 0, \dots, v - 1$	$\#JV - 2 - n$ $Vn = 0, \dots, v - 1$	WSWS	WS	$cr.^1$	$C_{ie,jV}$
2	HSHS	$\%v-1-n$ $Vn = 0, \dots, v - 1$	$XN-l-n$ $Vn = 0, \dots, v - 1$	WSWS	WS	C_s^{-1}	$C_{1e,jV+1}$
3	WSWA	$\%v - n$ $Vn = 0, \dots, v - 1$	$0, n = 0$ $-XN-l-n, n = 1, \dots, v - 1$	WSWA	WS	Cse^l	$C_{3e,iV}$
4	HSHA	$\%v-1-n$ $Vn = 0, \dots, v - 1$	$-XN-l-n$ $Vn = 0, \dots, v - 1$	WSWA	WS	$C \wedge^1$	$C_{3e,iV}$
5	WSHS	$\%v - n$ $Vn = 0, \dots, v - 1$	$Vn = 0, \dots, v - 1$	WSHS	WS	cro^1	$C_{io,jV}$
6	HSHS	$\%v-1-n$ $Vn = 0, \dots, v - 1$	$XN-2-n$ $Vn = 0, \dots, v - 1$	WSHS	WS	C_s^{-1}	$C_{io,jV}$
7	WSHA	$\%v - n$ $Vn = 0, \dots, v - 1$	$Vn = 0, \dots, v - 1$	WSHA	WS	c_{30}^1	$C_{30,iV}$
8	HSWA	$\%v-1-n$ $Vn = 0, \dots, v - 1$	$0, n = 0$ $-a^?jv-n? n = 1, \dots, v - 1$	WSHA	WS	c_{40}^1	$C_{30,N+1}$

HS

HS

WS

Therefore, it suffices to prove that

$$(C_2e^{\wedge}equiv)_k = (\wedge^2e)_{ko} (C_{ie,hzp})_k, \quad 1, \dots, iV.$$

So we just make the following computations:

$$(C_2eh_{equiv})_k$$

$$= 2 C_0 S \cdot 2W \cdot ho$$

$$2 C_0 S \cdot 2W \cdot ho + \mathbf{E}_{3=1}^{4hj \cos} \begin{matrix} kirj \setminus \\ \sim W \end{matrix} \cos \begin{matrix} (kir \\ [2N \end{matrix}$$

$$= (C_2e)_{fc} 0 (C_{1ehzp})_{fc} \cdot$$

Notice that the coefficients of each one-tap per subcarrier equalizer are obtained from the $(N + 1) \times 1$ column vector $C_{ie}h^{\wedge}p$. Therefore, the above results confirm what appears in [13]; moreover, they provide a direct and simpler way to get the coefficients of the one-tap per subcarrier equalizers.

B. DCT-III-Based MCM

The results obtained in [17] can also be deduced from Table III as follows:

- 1) For IDCT3e at the transmitter and DCT3e at the receiver. It corresponds to row 3 in Tables II and III. A whole-point symmetry (WS) on the left and a whole-point antisymmetry (WA) on the right have to be applied to the original symbol. Again in accordance with [16] for the FEQ block, d_i corresponds to the N -point DCT3e of h'_{zp} .
- 2) For IDCT3o at the transmitter and DCT3o at the receiver. It corresponds to row 7 in Tables II and III. A whole-point symmetry (WS) on the left and a half-point antisymmetry (HA) on the right have to be applied to the original data symbol. For the FEQ block, d_i corresponds to the iV -point DCT3o of h'_{zp} .

$$ML \quad JIi$$

$$A/-1 \quad -v \quad 0 \quad v$$

Fig. 3. Symmetries in x and h to turn the linear convolution into a symmetric convolution ($N > (2v + 1)$).

where H_{equiv} is the $V \times N$ equivalent channel matrix and e_i is the $N \times 1$ column vector that has a one in the i th position and zeros everywhere else.

Fig. 3 illustrates an example of the symmetries to be imposed on x and h to use the IDCT2e and the DCT2e as block transforms at the transmitter and the receiver sides, respectively. These transforms correspond to row 2 in Table III. This means the extension HS (see s_a) has to be introduced simultaneously as prefix and suffix into x . In addition, the front-end prefilter w has to obtain an equivalent impulse response h with symmetry WS (see first symmetry of S_b). Accordingly, the results in Table III perfectly match with those derived in [13], except for (1). It can be seen that the bank of scalars J , $0 < i < N - 1$, included in the FEQ block of Table III are obtained from the $(N + 1)$ -point DCT Type-I even ($C_{ie}Ar+i$) of the impulse response h'_{zp} , whereas in [13], Al-Dhahir *et al.* show that d_i are given by (1), which can be expressed as

$$0, \quad , iV - 1, \quad (2)$$

where the $N \times 1$ column vector h_{equiv} is the first column of H_{equiv} defined in [13] as

$$[h_0 + h, \quad hi + /i_2, \quad h_v-i + h_v, \quad h_v, \quad 0 \quad \mathbf{o}]^T.$$

Next, we demonstrate that both (1), (2) are equivalent to the result shown in Table III, i.e., d_i corresponds to the discrete cosine transform type-I (DCT1) of the filter $\setminus i'_{zp}$ ³

$$d_i = (\wedge^2e^{\wedge}equiv)_{jix} = (C_{1e}h^r_{zp})_{i+1}, \quad i = 0, \dots, iV - 1,$$

³Remark that in this case h'_{zp} is extended by zero-padding to $N + 1$ samples.

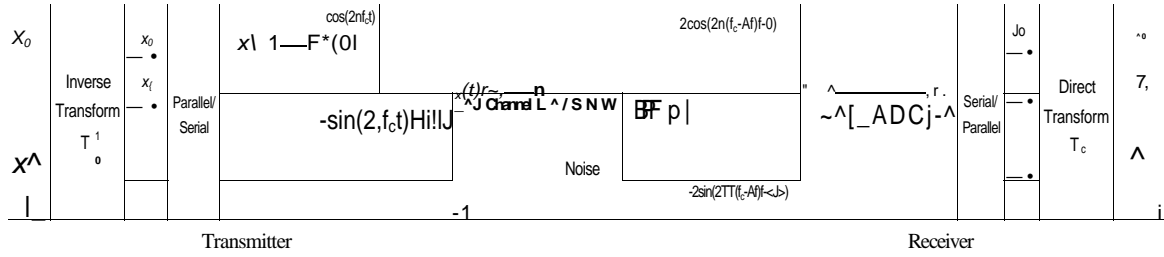


Fig. 4. Block diagram of a multicarrier modulation system in the presence of CFO.

TABLE IV
SIMULATION PARAMETERS

Parameters	Value
Modulation and Demodulation	QPSK
Subcarrier Number	128
Channel Model	SUI-5 [20]
Noise Model	iid AWGN
Doppler Spectrum	Round, Classic and Flat
Lengths of Cyclic, Right, and Left Prefixes	32
Normalized Carrier Frequency Offsets (A/T)	0.02, 0.1

IV. EXAMPLE DESIGN

In this section, we evaluate and compare by computer simulations the performance of the DFT-MCM and the DCT4e-MCM introduced earlier, also considering the impact of CFO on the bit error rate. A comparison between the DFT-MCM systems and the rest of DCT-MCM has not been included in this work because the simulation results show identical bit error rate (BER) performances for every kind of DCT (I, II, III and IV, even and odd) in all the communication scenarios herein considered.

The block diagram of the system used for the simulations is depicted in Fig. 4. It includes in-phase and quadrature modulators in the presence of CFO (A/T). More than five million binary data were generated and converted into parallel data to be transmitted over one hundred and twenty-eight subcarriers. Before proceeding with the multicarrier modulation, the data at each subcarrier are mapped by QPSK modulation. After mapping them, the parallel data were fed into the inverse block transform at the transmitter, considering the IFFT and the IDCT4e in order to compare their performances. The parameters used for the simulations are summarized in Table IV.

We consider as transmission scheme a high speed vehicle channel with high delay spread—the power delay profile of channel SUI-5 in [20]—considering the three kinds of Doppler spectrum aforementioned: round, classic and flat. The speed of the mobile was chosen to have a channel coherence time of similar value as the OFDM and DCT4 symbol periods. The value of the ratio bandwidth/channel sampling rate was one. At the receiver, perfect timing synchronization and channel estimation is assumed, and the front-end prefilter is implemented as the *time-reversed* (matched) filter to the estimated channel. In addition, in order to perform the frequency-domain equalization, the zero-forcing equalizers are used for each corresponding channel.

In Fig. 5 we present the results obtained with the mobile channel and round Doppler spectrum for several frequency offsets. It can be seen that the curves of the error probability versus E_b/N_0 acquire the linear shape of the Rayleigh channel, and that the DCT4e-MCM system is more robust than OFDM against frequency offsets. In fact, when the offset $A/T = 0.1$ the latter reaches an error floor at $p = 25$ dB while the former error probability continues lowering with increasing signal noise ratio (SNR).

We have also studied the effect of the shape of the Doppler spectrum over the error probability. In Figs. 6 and 7 we present the results obtained with the OFDM and DCT4e-MCM systems, operating in chan-

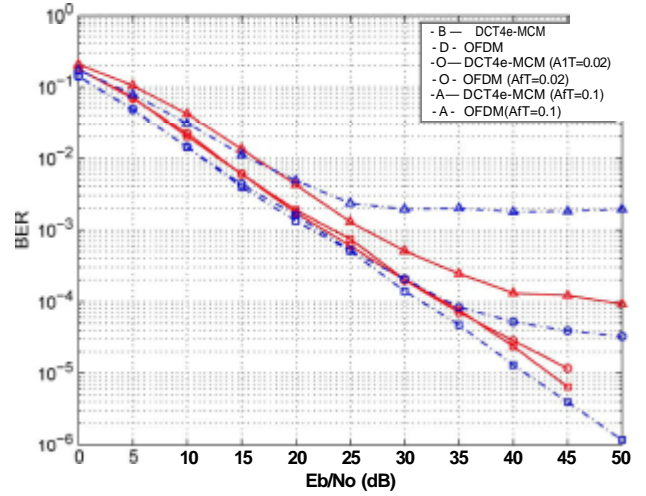


Fig. 5. Results obtained for DFT-MCM and DCT4e-MCM transmissions in a high speed and multi-path mobile channel in the presence of frequency offset ($N = 128$, QPSK, and $A/T = 0.02, 0.1$). The Doppler spectrum is round.

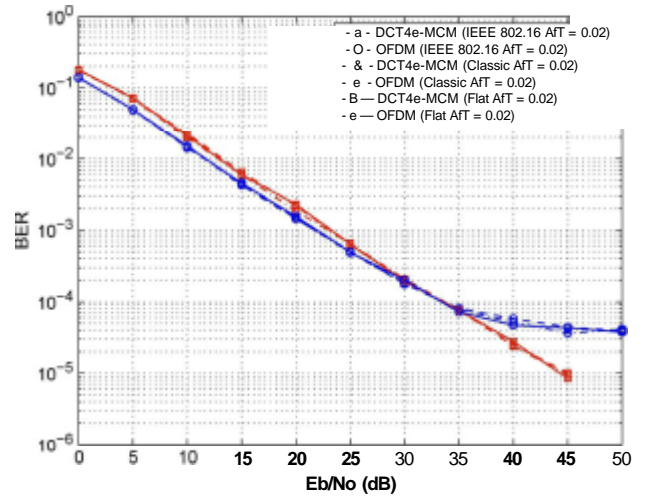


Fig. 6. Results obtained for DFT-MCM and DCT4e-MCM for a multi-path mobile channel with round, flat and classic Doppler spectrum. The frequency offset is $A/T = 0.02$ and $N = 128$, QPSK.

nels with the three aforementioned Doppler spectra and the normalized frequency offsets $A/T = 0.02$ and $A/T = 0.1$. A first result is that the shape of the spectrum has little impact on the error probability. However, the flat spectrum is usually a worst-case scenario. Both systems have error floor, but the floor of the system DCT4e-MCM is lower by one order of magnitude. Even more, the error floor of the DCT4e-MCM system is reached with a SNR value 15 dB larger than the corresponding to the floor of the OFDM system. This confirms that DCT4e-MCM outperforms OFDM in the presence of CFO.

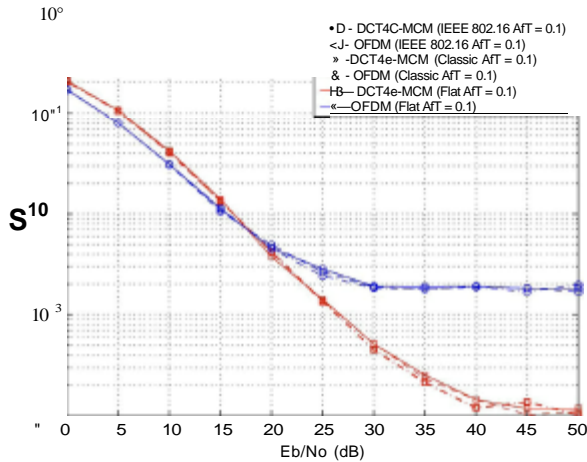


Fig. 7. Results obtained for DFT-MCM and DCT4e-MCM for a multi-path mobile channel with round, flat and classic Doppler spectrum. The frequency offset is $AfT = 0.1$ and $N = 128$, QPSK.

V. CONCLUSIONS

In this work, the application of DCTs for multicarrier communications has been addressed. We have shown that the transmitter of each system includes an inverse DCT and a parallel-to-serial converter in which a prefix and a suffix are introduced into the data symbol to be transmitted. The receiver consists of a front-end prefilter plus another DCT. We have obtained the conditions to use any kind of DCT for multicarrier data transmission based on the fact that DCTs have the convolution-multiplication property, that is, a symmetric convolution in the time-domain is transformed in an element-by-element multiplication in the corresponding discrete cosine transform domain. The configuration of both the transmitter and the receiver, the symmetry to be imposed by the front-end prefilter, and the prefix and the suffix to be appended into each data symbol, have been established for the eight different types of DCTs. Furthermore, the values of the coefficients for the one-tap per subcarrier equalizer have also been provided. Finally, the simulation results have verified that DCT-MCM outperforms OFDM in different scenarios in the presence of CFO.

ACKNOWLEDGMENT

The authors would like to thank the Associate Editor and the anonymous Reviewers for their insightful recommendations, which have significantly contributed to the improvement of this paper.

REFERENCES

- [1] J. A. C. Bingham, "Multicarrier modulation for data transmission: An idea whose time has come," *IEEE Commun. Mag.*, vol. 28, no. 5, pp. 5-14, May 1990.
- [2] *Digital Video Broadcasting (DVB); Frame Structure, Channel Coding and Modulation for a Second Generation Digital Terrestrial Television Broadcasting System (DVB-T2)*, ETSI EN 302 755, V1.2.1, European Telecommunications Standards Institute, Feb. 2011.
- [3] *Wireless LAN Medium Access Control (MAC) and Physical Layer (PHY) Specifications: Enhancement for Higher Throughput*, IEEE Standard 802.11n, 2009.
- [4] *IEEE Standard for Broadband Over Power Line Networks: Medium Access Control and Physical Layer Specifications*, IEEE Standard 1901.2010, Dec. 2010.
- [5] *Very High Speed Digital Subscriber Line 2 (VDSL2)*, ITU-T Recommendation G.993.2, 2006.

- [6] *IEEE Standard for Local and Metropolitan Area Networks, Part 16: Air Interface for Broadband Wireless Access Systems*, IEEE Standard 802.16e, May 2009.
- [7] *Evolved Universal Terrestrial Radio Access (E-UTRA); Physical Channels and Modulation*, 3 GPP, TS 36.211, v 8.4.0, 3 GPP Technical Specification, Sep. 2008.
- [8] *IEEE Standard for Information Technology-Telecommunications and Information Exchange Between Systems-Local and Metropolitan Area Networks-Specific Requirements Part 11: Wireless LAN Medium Access Control (MAC) and Physical Layer (PHY) Specifications Amendment 6: Wireless Access in Vehicular Environments*, IEEE Standard 802.16p, IEEE Standard 802.11p-2010 (Amendment to IEEE Standard 802.11-2007 as amended by IEEE Standard 802.11k-2008, IEEE Standard 802.11r-2008, IEEE Standard 802.11y-2008, IEEE Standard 802.11n-2009, and IEEE Standard 802.11w-2009), Jul. 2010.
- [9] V. Sanchez, P. Garcia, A. M. Peinado, J. C. Segura, and A. J. Rubio, "Diagonalizing properties of the discrete cosine transforms," *IEEE Trans. Signal Process.*, vol. 43, no. 11, pp. 2631-2641, Nov. 1995.
- [10] S. Attallah and J. E. M. Nilsson, "Sequences leading to minimum peak-to-average power ratios for DCT-based multicarrier modulation," *Electron. Lett.*, vol. 34, no. 15, pp. 1469-1470, Jul. 23, 1998.
- [11] J. Tan and G. L. Stüber, "Constant envelope multi-carrier modulation," in *Proc. MILCOM*, Oct. 7-10, 2002, pp. 607-611.
- [12] G. D. Mandyam, "Sinusoidal transforms in OFDM systems," *IEEE Trans. Broadcast.*, vol. 50, no. 2, pp. 172-184, Jun. 2004.
- [13] N. Al-Dhahir, H. Minn, and S. Satish, "Optimum DCT-based multicarrier transceivers for frequency-selective channels," *IEEE Trans. Commun.*, vol. 54, no. 5, pp. 911-921, May 2006.
- [14] P. Tan and N. C. Beaulieu, "A comparison of DCT-based OFDM and DFT-based OFDM in frequency offset and fading channels," *IEEE Trans. Commun.*, vol. 54, no. 11, pp. 2113-2125, Nov. 2006.
- [15] F. Gao, T. Cui, A. Nallanathan, and C. Tellambura, "Maximum likelihood based estimation of frequency and phase offset in DCT OFDM systems under non-circular transmissions: Algorithms, analysis and comparisons," *IEEE Trans. Commun.*, vol. 56, no. 9, pp. 1425-1429, Sep. 2008.
- [16] S. A. Martucci, "Symmetric convolution and the discrete sine and cosine transforms," *IEEE Trans. Signal Process.*, vol. 42, no. 5, pp. 1038-1051, May 1994.
- [17] M. E. Dominguez Jimenez, G. Sansigre Vidal, P. Amo-López, and F. Cruz-Roldan, "DCT3 for multicarrier communications," presented at the 19th Eur. Signal Process. Conf. (EUSIPCO), Barcelona, Spain, Aug. 29-Sep. 2, 2011.
- [18] X. Zhao, J. Kivinen, and P. Vainikainen, "Characterization of Doppler spectra for mobile communications at 5.3 GHz," *IEEE Trans. Veh. Technol.*, vol. 52, no. 1, pp. 14-22, Dec. 2003.
- [19] R. K. Martin, K. Vanbleu, M. Ding, G. Ysebaert, M. Milosevic, B. L. Evans, M. Moonen, and C. R. Johnson, Jr., "Implementation complexity and communication performance tradeoffs in discrete multitone modulation equalizers," *IEEE Trans. Signal Process.*, vol. 54, no. 8, pp. 3216-3230, Aug. 2006.
- [20] *Channel Models for Fixed Wireless Applications*, IEEE 802.16, Broadband Wireless Access Working Group, Jul. 2001.